MONITORING SURFACE DEFORMATION ASSOCIATED WITH GROUNDWATER ABSTRACTION IN THE WESTERN CAPE USING SAR INTERFEROMETRY

Mr, A, Theron

CSIR, Meraka Institute, Stellenbosch

Stellenbosch University, Department of Geography and environmental studies, Stellenbosch

Dr, J, Engelbrecht

CSIR, Meraka Institute, Stellenbosch

Stellenbosch University, Department of Geography and environmental studies, Stellenbosch

Corresponding Author:

Mr, A, Theron

CSIR Jan Celliers road, Stellenbosch Central, Stellenbosch, 7600

Telephone number: 021 888 2453

E-mail address: Atheron1@csir.co.za

Keywords: Remote sensing, Groundwater, Drought, SAR, Interferometry

Geoinformatics: Remote sensing

MONITORING SURFACE DEFORMATION ASSOCIATED WITH GROUNDWATER ABSTRACTION IN THE WESTERN CAPE USING SAR INTERFEROMETRY

ABSTRACT

Aquifers are able to contain significant amounts of water, which is typically stored in the pore spaces between sand particles or in the fissures and matrix of rocks. This groundwater is an increasingly important source of water in many parts of South Africa, particularly along the arid south-west coast where the relatively deep (<150m) Elandsfontein and Langebaan road aquifers are found. Groundwater is extracted here for agriculture, industry and domestic use. Recent borehole data shows that increased abstraction combined with the low rainfall experienced between 2015 and 2018 is resulting in reduced groundwater levels in the area. Groundwater abstraction may lead to ground subsidence due to pressure reduction and can lead to permanent storage potential loss due to compaction. Ground surface monitoring is therefore valuable for sustainable aquifer management, preventing damage to infrastructure and providing input to geo-hydrological models. Such monitoring can be done with differential-GPS or levelling surveys but these are labour-intensive, expensive and do not provide comprehensive spatial coverage of an aquifer. Synthetic Aperture Radar (SAR) is an active remote sensing system capable of imaging the earth in the microwave spectrum and capturing both the intensity and phase of the returning signal. Comparing the phase of the same surface over time with a technique called differential interferometry (DInSAR) allows spatial monitoring of earth surface movements to fractions of a wavelength (mm to cm). This work investigates DInSAR monitoring of the south-west coast using Sentinel-1 C-band data in an attempt to detect small-scale ground subsidence over large areas. Early results show that Sentinel-1 is an appropriate data source. However, limitations inherent to conventional DInSAR techniques were encountered namely: 1) the dynamic land-cover of the study area, 2) the slow deformation rate and 3) atmospheric noise similar in scale to the expected deformation. Advanced time-series approaches are recommended for effective monitoring of aquifer related deformation in the area.

1. INTRODUCTION

Aquifers are able to contain significant amounts of water, which is typically stored in the pore spaces between sand particles or in the fissures and matrix of rocks. Groundwater can be abstracted from aquifers for residential, agricultural or industrial use and is replenished again from recharge, either naturally through rainfall and streamflow or by borehole injection (Department of Water Affairs 2009). Drought conditions or over abstraction can lead to lowered water levels and can result in ground subsidence due to pressure reduction (Armas *et al.* 2017). Subsidence can be a hazard to infrastructure and lead to permanent storage potential loss due to aquifer compaction. Deformation relating to aquifer abstraction is expected to be relatively small in magnitude, with typical rates in the order of centimetres per year. On the other hand, the extent of deforming areas are large in scale with deformation basins expected to be hundreds of meters and up to kilometres wide (Chen et al. 2016). Measuring such deformation is very challenging using conventional *in situ* methods, however, remote sensing techniques have become available that can exploit the synoptic view and frequent revisit of satellite platforms to provide small scale deformation measurements (Wang *et al.* 2018). A widely used technique is called Differential Synthetic Aperture Radar Interferometry (DInSAR) which allows the monitoring of earth surface for deformation in the scale of millimetres. This study aimed to investigate the potential of DInSAR using Sentinel-1 medium resolution, c-band radar data to measure surface deformation related to groundwater abstraction over two important west coast aquifers during the 2015 to 2018 drought

2. AQUIFERS AND GROUND DEFORMATION MONITORING

Aquifers are important sources of water across the world and are often exploited, particularly during dry periods, when surface water becomes scarce (Western Cape Department of Agriculture 2017). Aquifers are geological formations able to hold water or permit appreciable water movement through them (South Africa 1998). Groundwater can be found in the fissures and matrix off hard rock formations as well as between the sand grains found in coastal, river and wind-blown environments. In South Africa groundwater is typically found in rock formations (90%) as opposed to sand (10%) (Department of Water Affairs 2009). Groundwater cannot evaporate, but may be lost through pumping, spring flows and evapotranspiration via plants. Aquifers are recharged naturally when water on the ground infiltrate the soil profile and ultimately saturate fissures in hard rocks or the openings between sand grains. Aquifers can also be recharged through artificial injection (Niu *et al.* 2017).

Ground deformation due to groundwater dynamics may occur in confined or unconfined aquifers but the relationship is particularly evident for confined aquifers, which are pressurised systems, where a change in water pressure can often be directly related to ground surface deformation (Amos *et al.* 2014; Chen *et al.* 2016; Armas *et al.* 2017). The relationship is more complicated for unconfined aquifers (Motagh *et al.* 2017; Rezaei 2018). Aquifers containing fine-grained silt and clay are prone to permanent subsidence and a reduction in water storage potential due to inelastic compaction. Elastic compaction, which results in smaller, temporary, surface subsidence, is characteristic of course grained sand and gravel deposits (Amelung *et al.* 1999). Aquifers behaving elastically can be abstracted from and then restored to their original state through artificial or natural recharge (Matthews 2014). Subsidence measurements over certain aquifers can therefore be used to aid in calculating their storage potential (Wang *et al.* 2018). Furthermore, subsidence induced by a lowering of the water table can result in geo-hazards such as induced seismicity, sinkholes or infrastructure damage (Amos *et al.* 2014; Alfarrah *et al.* 2017).

Much of the recent evidence for aquifer related deformation has been collected by DInSAR (Bell *et al.* 2008; Radutu *et al.* 2017), a remote sensing technique capable of measuring sub-millimetre changes of the earth's surface over time (Ferretti *et al.* 2007). Such measurements are made possible by the characteristics of SAR imaging systems. SAR sensors are active systems that emit and receive microwaves with typical wavelengths between 3 cm and 25 cm. The system is therefore independent of natural light sources. Furthermore, microwaves are able to penetrate cloud and even certain vegetation canopies (Hanssen 2001). A SAR system records the amplitude as well as the phase of the returning microwave pulse. The phase is directly related to a change in distance between the radar and the surface and can be measured very accurately to a few millimetres. DInSAR relies on comparing the returning phase from the same area imaged over different times (the amount of days between acquisitions is called the temporal baseline) to provide an accurate measurement of the change in the distance between the SAR platform and the ground surface (Ferretti *et al.* 2007). Conventional repeat-pass interferometry uses two scenes, but advanced approaches have been developed which makes use of time-series stacks to improve the deformation estimate (Hooper *et al.* 2004; Ferretti *et al.* 2011).

3. STUDY SITE

The proposed study area to be investigated is the Langebaan road and Elandsfontein aquifers found along the plains of the South Africa's southwestern coast shown in Figure 1. Groundwater is an important source of water for the area and is used for residential, mining, industrial and agricultural use. Groundwater is widely used and increased groundwater abstraction is planned (Western Cape

Department of Agriculture 2017). Groundwater is fed from a wellfield in the Langebaan Road aquifer to the towns in the region including Langebaan, Saldanha and Vredenburg. Figure 1 shows the location of the monitoring boreholes maintained by the Department of Water and Sanitation. The area is being investigated for water storage through artificial injection as part of a Managed Aquifer Recharge (MAR) scheme (Department of Water Affairs 2009). Furthermore, an open pit phosphate mine recently started operating in the Elandsfontein aquifer region and, to avoid contamination the mine aims to divert groundwater around the site by abstraction and artificial injection (Pepler 2013). Granite outcroppings are found in the region; these are not expected to be prone to surface deformation over the course of this study and can therefore be used as stable reference points for DInSAR measurements (Parker, Filmer & Featherstone 2017). Figure 1 shows the location of the reference point used for this study. The majority of the study area is dominated by agriculture. Agricultural fields are typically not irrigated, however, some centre pivot plots utilizing groundwater are found in the area. Natural vegetation found here is typically small to medium sized shrubs. The region receives on average ~300 mm of winter rainfall.

Figure 1: The study area showing the approximate extent of the Langebaan road and Elandsfontein aquifers as well as the boreholes and stable reference point used in this study.

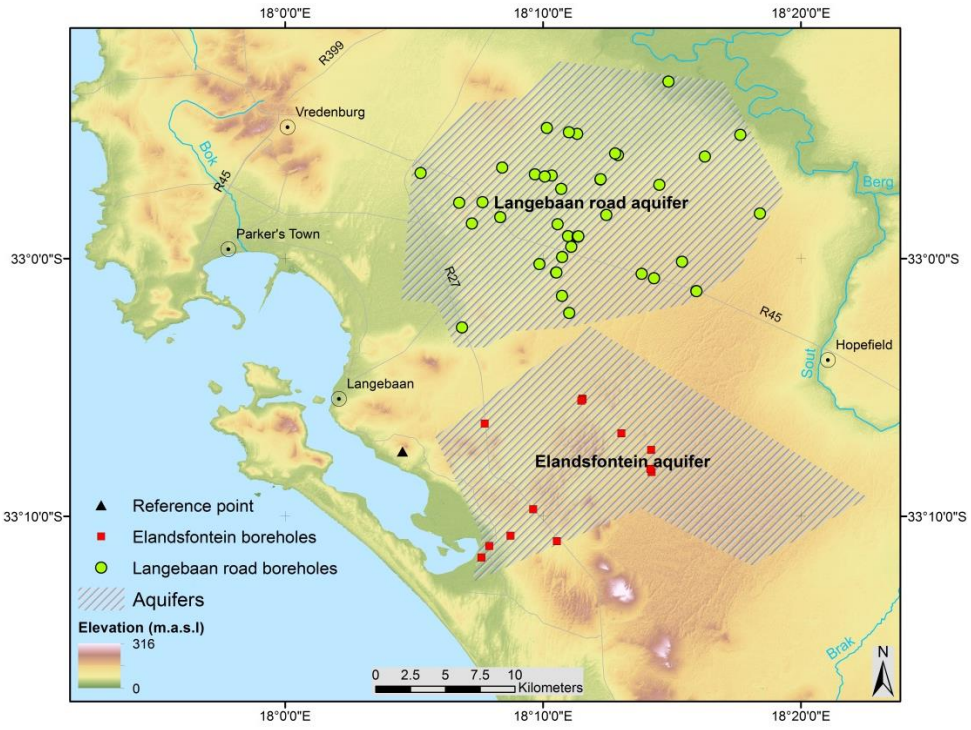

Source: Aquifer and borehole data provided by the Department of Water and Sanitation.

The Langebaan road and Elandsfontein aquifers are the main aquifers of interest in this study. They are sandy aquifers, as opposed to fractured rock aquifers. Their structures generally consist of a lower and upper aquifer separated by a clay layer. The clay layer is not continuous and groundwater flow through the discontinuities is likely, yet not well understood. The lower aquifer is a semi-confined aquifer due to the underlying basement granites of the Malmesbury group and the clay layer above it. Both aquifers drain through the sandy geology towards the south-west, following the paleo-channel basement rock topography (Pepler 2013). The aquifers are possibly hydrologically connected, with linkages between both the two neighbouring aquifers as well as between the lower and upper aquifers (Du Plessis 2009). Factors that increase the likelihood for ground deformation as a result of groundwater level dynamics over these aquifers are that they are relatively deep (<150m), intergranular and contained in places by a clay layer.

There is evidence that the groundwater level for the area has lowered during the 2015 to 2017 drought. A number of research boreholes have been drilled in the area by the Department of Water and Sanitation (DWS) in the early 1980s (locations depicted in Figure 1). More than 60% of these boreholes showed declining water levels since 2015 (Western Cape Department of Agriculture 2017). Figure 2 shows the annual departure from the long-term average of each borehole, averaged over all the boreholes. Using water level anomaly allows for the averaging of borehole data with different absolute water levels and responses. The historical water levels from these boreholes show that groundwater levels respond to annual rainfall variability, and the recent 2015 to 2017 drought periods can be seen as consecutive negative water level anomalies in Figure 2. The difference in water levels between the 1980 to 1991 and 2000 to 2017 periods can be explained in part by the introduction of electricity and increased population and water use activities resulting in increased groundwater pumping. No data was captured between 1992 and 1999 and data for 2018 unavailable at the time of publication.

Figure 2: Average annual groundwater level anomalies for the DWS boreholes relative to the 1980-2017 mean. The effect of dry periods can be seen, particularly the most recent 2015 to 2018 drought.

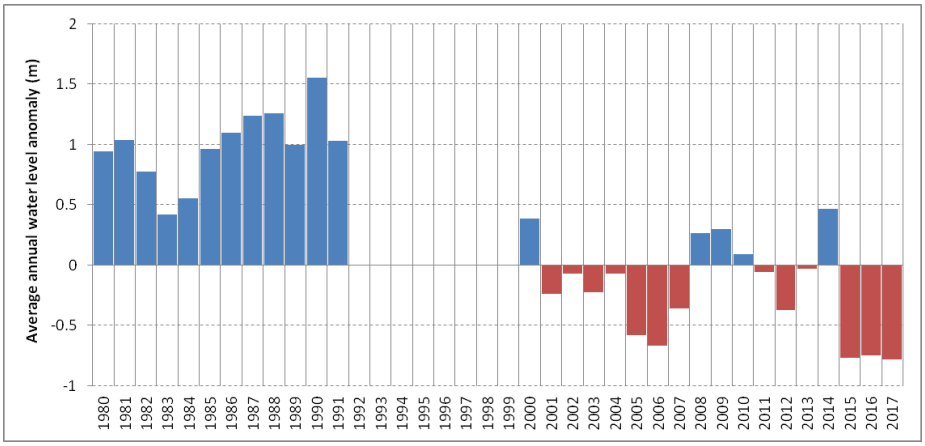

Source: Department of water and sanitation (2017)

4. PROBLEM STATEMENT AND METHODS

SAR interferometry has not been used to measure deformation over the West Coast aquifers, even though it has been widely used for this application in other parts of the world (Radutu *et al.* 2017). It is not known whether significant deformation has, or is, taking place over the Langebaan road and Elandsfontein aquifers. Deformation due to groundwater level change can be expected here due to the geological properties of the aquifers and the lowered water level due to the low rainfall and increased abstraction during the 2015 to 2018 period. It is however expected to be challenging to detect such deformation using conventional repeat-pass interferometry since aquifer related deformation typically occurs at relatively large scales, over hundreds of meters, and small magnitudes, a few centimetres per year. Repeat-pass interferometry is suited for monitoring rapid, large magnitude deformation events such as earthquakes and volcanic activity (Hanssen 2001). Advanced time-series stacking techniques (Ferretti *et al.* 2011) are instead used for aquifer related deformation (Radutu *et al.* 2017). These however require complex and computationally intensive processing. It is therefore worthwhile to attempt to generate a time-series through repeat-pass interferometry before investigating the more advanced approaches.

The objective of this paper was to test the ability to reliably measure deformation rate and magnitude over the west-coast aquifers by using repeat-pass interferometry. This was done by 1) selecting data to minimise the duration between image acquisitions (temporal baselines), 2) maximising the observation period, 2) adaptive spatial filtering and multi-looking (subsampling) the data to a lower spatial resolution to reduce phase noise, 3) inspecting and discarding scenes that did not unwrap successfully

(see Section 4.2), 4) extracting the deformation only from points likely to show deformation and 5) Masking the points without a coherent phase return over specific interferometric pairs.

4.1.Data

The primary data used for this study was level-1 Single Look Complex (SLC) Sentinel-1 imagery that was obtained from the European Space Agency (Copernicus Sentinel data 2018). 54 images were used for this study beginning from 2015/11/19 up to 2018/04/01 with a minimal revisit time between acquisitions of 12 days. See Table 1 for the specific dates and revisit times. Data was captured using the Interferometric Wide (IW) swath mode which uses a scanning technique that combines multiple smaller "bursts" into three sub-swaths to form a single image covering an area 250 km wide at a resolution of approximately 4 m in range (across-track) at 14 m in azimuth (along-track) (Grandin 2016). Table 1 also shows the day difference between acquisitions (temporal baseline) and the separation between orbits (perpendicular baseline). The perpendicular baseline is important since a large baseline (in the order of hundreds of meters) results in the phase being sensitive to varying topography as well as deformation, which complicates deformation analysis. Table 1 also shows which image pairs were discarded after visual quality check and the offset that was applied to each scene based on the stable reference point (explained in section 4.2).

Table 1: Properties of the Sentinel-1 dataset used for this study.

Master date	Slave date	Temporal Baseline (days)	Perpendicular baseline (m)	Quality check	Reference Offset (m)	Master date	Slave date	Temporal Baseline (days)	Perpendicular baseline (m)	Quality check	Reference Offset (m)
2015/11/19	2015/12/01	12	-61	pass	-0.0159	2017/05/12	2017/05/24	12	43	pass	-0.0032
2015/12/01	2015/12/13	12	-76	fail	n/a	2017/05/24	2017/06/05	12	-6	pass	0.0016
2015/12/13	2016/01/06	24	108	pass	-0.0015	2017/06/05	2017/06/17	12	67	pass	0.0180
2016/01/06	2016/01/30	24	50	pass	-0.0262	2017/06/17	2017/06/29	12	1	pass	0.0064
2016/01/30	2016/02/23	24	-114	pass	0.0131	2017/06/29	2017/07/11	12	-34	pass	0.0086
2016/02/23	2016/03/18	24	79	fail	n/a	2017/07/11	2017/07/23	12	-1	pass	0.0065
2016/03/18	2016/03/30	12	28	fail	n/a	2017/07/23	2017/08/04	12	-49	pass	-0.0050
2016/03/30	2016/04/11	12	19	pass	0.0049	2017/08/04	2017/08/16	12	76	pass	0.0162
2016/04/11	2016/04/23	12	62	fail	n/a	2017/08/16	2017/08/28	12	-25	pass	0.0104
2016/04/23	2016/05/05	12	22	pass	0.0187	2017/08/28	2017/09/09	12	-25	pass	0.0094
2016/05/05	2016/05/17	12	39	pass	-0.0173	2017/09/09	2017/09/21	12	-22	fail	n/a
2016/05/17	2016/06/10	24	11	pass	-0.0028	2017/09/21	2017/10/03	12	37	fail	n/a
2016/06/10	2016/11/13	156	-70	fail	n/a	2017/10/03	2017/10/15	12	16	fail	n/a
2016/11/13	2016/11/25	12	7	pass	0.0109	2017/10/15	2017/10/27	12	-24	pass	-0.0083
2016/11/25	2016/12/07	12	19	pass	0.0127	2017/10/27	2017/11/08	12	24	pass	-0.0091
2016/12/07	2016/12/19	12	-15	fail	n/a	2017/11/08	2017/11/20	12	-63	pass	-0.0193
2016/12/19	2016/12/31	12	-87	pass	-0.0044	2017/11/20	2017/12/02	12	38	pass	0.0101
2016/12/31	2017/01/12	12	23	pass	0.0040	2017/12/02	2017/12/14	12	14	pass	-0.0096
2017/01/12	2017/01/24	12	74	pass	-0.0066	2017/12/14	2017/12/26	12	71	pass	0.0128
2017/01/24	2017/02/05	12	22	pass	0.0006	2017/12/26	2018/01/07	12	-53	fail	n/a
2017/02/05	2017/02/17	12	50	pass	0.0059	2018/01/07	2018/01/19	12	-86	pass	-0.0061
2017/02/17	2017/03/13	24	-116	pass	0.0082	2018/01/19	2018/01/31	12	38	fail	n/a
2017/03/13	2017/03/25	12	44	pass	-0.0127	2018/01/31	2018/02/12	12	-18	pass	-0.0078
2017/03/25	2017/04/06	12	34	pass	0.0062	2018/02/12	2018/02/24	12	117	pass	0.0048
2017/04/06	2017/04/18	12	4	pass	0.0247	2018/02/24	2018/03/08	12	49	pass	0.0178
2017/04/18	2017/04/30	12	-9	fail	n/a	2018/03/08	2018/03/20	12	-52	fail	n/a
2017/04/30	2017/05/12	12	-84	fail	n/a	2018/03/20	2018/04/01	12	-76	fail	-0.0187

4.2.Methods

Data processing followed the standard repeat-pass interferometry workflow using the Gamma Remote Sensing SAR processor outline in the workflow in Figure 3 (Wegmüller *et al.* 2015). The image metadata is first updated with precise orbital state vectors. Sequential images were then used as master and slave images to minimise the day difference between scenes and ensure the entire study period is covered. Image co-registration was done as a two-step process by performing intensity cross correlation using the amplitude data as a first step, and then performing the enhanced spectral diversity method that makes use of the phase information at burst overlap regions to achieve co-registration accuracy of 0.0001 pixels (Grandin 2016).

Figure 3: Repeat-pass interferometric workflow used to generate displacement maps.

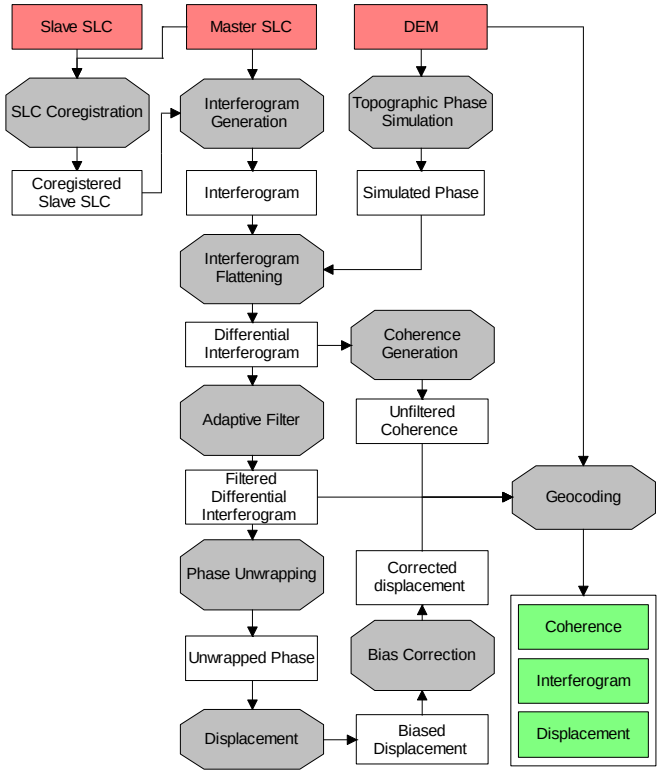

Source: Theron (2017)

The master and slave scenes are then cross-multiplied to form an interferogram. SAR pixels have different dimensions along and across-track and images were therefore multi-looked (under-sampling factors: along-track=15, across-track=4) during this step resulting in square pixels with 56 m resolution. The SRTM 1 arc (under-sampled to 56 m) digital elevation model was used to remove phase contributions from "flat earth" and topography resulting in a differential interferogram and a coherence map. Coherence is a measure of phase stability between acquisitions and is a useful indicator of phase measurement quality (Engelbrecht & Inggs 2016). The Interferogram was then filtered using the Goldstein filter which adaptively changes the window size depending on the local coherence, with stronger filtering applied to lower coherence areas (Goldstein & Werner 1998).

The interferogram phase was then unwrapped using a minimum cost flow algorithm which converts the phase from radians to meters (Costantini 1998). The relative vertical displacement component is then extracted from the line of sight observation, since the radar is side looking, under the assumption that all displacement measured is vertical. The unwrapped images were then visually inspected for unwrapping errors, these were easily seen as artificial artefacts, or "islands" where the deformation

estimate steps up by tens of centimetres between rows of pixels. They are typically the result of too much phase noise in the interferogram and cannot be easily corrected. 15 out of the 54 scenes showed such artefacts across the study area and where discarded. The final list of pairs used in the analysis is provided in Table 1.

Relative displacement was then converted to absolute displacement by subtracting an offset for each image (Parker, Filmer & Featherstone 2017). The offset for each pair is in Table 1. The offset was estimated by using a point that is close to the area of interest, that likely underwent no deformation during the study period and that displayed a consistently high degree of coherence. The reference point chosen for this study was Granite bedrock outcropping located at 18.0767 E, 33.122 S in the West Coast nature reserve (black triangle in Figure 1).

Finally, the deformation history was then extracted for all the Department of Water Affairs borehole locations found in Langebaan road and Elandsfontein aquifers to assess and compare the rate and total magnitude of deformation (see the boreholes mapped in Figure 1). This sampling strategy ensures that deformation is measured over areas where there is evidence of substantial groundwater. There were 13 boreholes in the Elandsfontein and 43 in the Langebaan road aquifer. To ensure reliable deformation histories only points were extracted with a corresponding coherence higher than 0.3.

5. RESULTS AND FINDINGS

An example of an interferogram generated for the period between 2017/06/05 and 2017/06/17 is provided in Figure 4. The strong radar returns of the towns, the geometric shapes of agricultural fields and the average return of the natural vegetation in the centre of the scene is seen in the calibrated backscatter scene that is included for orientation (Figure 4A). The scene coherence (Figure 4B) shows the bright, highly coherent return from the urban areas, some low coherence agricultural fields (dark shades) that were likely disturbed between image acquisitions and the intermediate coherence for the natural vegetation in the centre and lower parts of the image.

Figure 4: Example of master scene backscatter (A), coherence (B), interferogram (C) and vertical displacement (D) for the study area for the 2017/06/05 to 2017/06/17 interferometric pair.

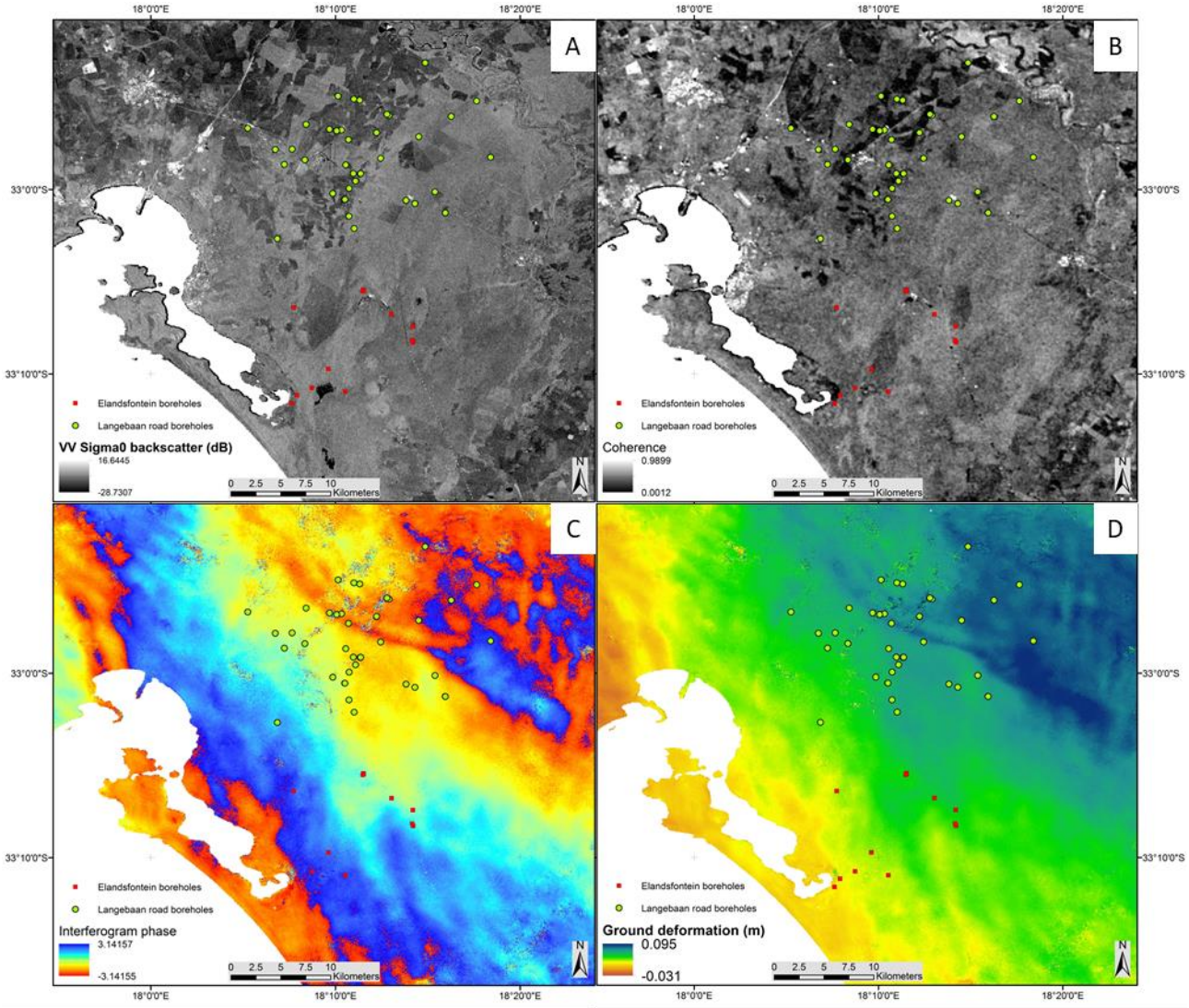

The interferogram (Figure 4C), typical of the data stack, represents a change in phase between image acquisitions and is measured in angles (between –pi and +pi). Residual topography, often a problem due to topographic phase correction errors, is not very prominent due to the low perpendicular baseline (67 m) and the low relief of the study area. This interferogram shows some smaller fringe patterns in the top right of the scene that is likely due to atmospheric conditions. Water vapour may result in a signal delay that can often be confused with a deformation signal (Hanssen 2001). There are also lower frequency fringes crossing from the top left to the bottom right closer to the coastline that could be due to atmosphere or incorrect satellite orbital information. Phase noise can also be seen over the

agricultural fields with very low coherence (Engelbrecht & Inggs 2016). No clear fringes are seen over the aquifers under investigation.

The vertical displacement map (Figure 4D) calculated from unwrapping the interferogram shows a deformation range of -0.031 m to 0.095 m. The deformation measurement follows the interferogram patterns and the noisy areas over the agricultural fields can still be seen. The apparent uplift of up to 9.5 cm at the top right of the scene is likely not caused by ground deformation but rather by atmospheric artefacts identified on the interferogram. Note that the borehole locations for the Langebaan road aquifer are in between the agricultural fields while the Elandsfontein boreholes are located over natural vegetation.

The deformation histories for the points were extracted and cumulatively added over the time-series between 2015/11/19 and 2018/04/01 to determine the deformation measured and provide a comparison between aquifers. The cumulative deformation is summarised graphically in Figure 5. The total deformation recorded was -0.006 m and -0.024 m for the Elandsfontein and Langebaan Road aquifers respectively. No linear trend with a reliable R^2 value could be found throughout the total study period. Although it is possible that seasonal trends can be present, they would need to be investigated further by incorporating the rainfall and water level data. Furthermore, the only clear differences between aquifers seem to be that Langebaan Road has a higher variance.

Figure 5: Cumulative displacement of the Langebaan road and Elandsfontein aquifers between 2015/11/19 and 2018/02/24 measured over the department of water affairs boreholes by DInSAR using Sentinel-1 Data.

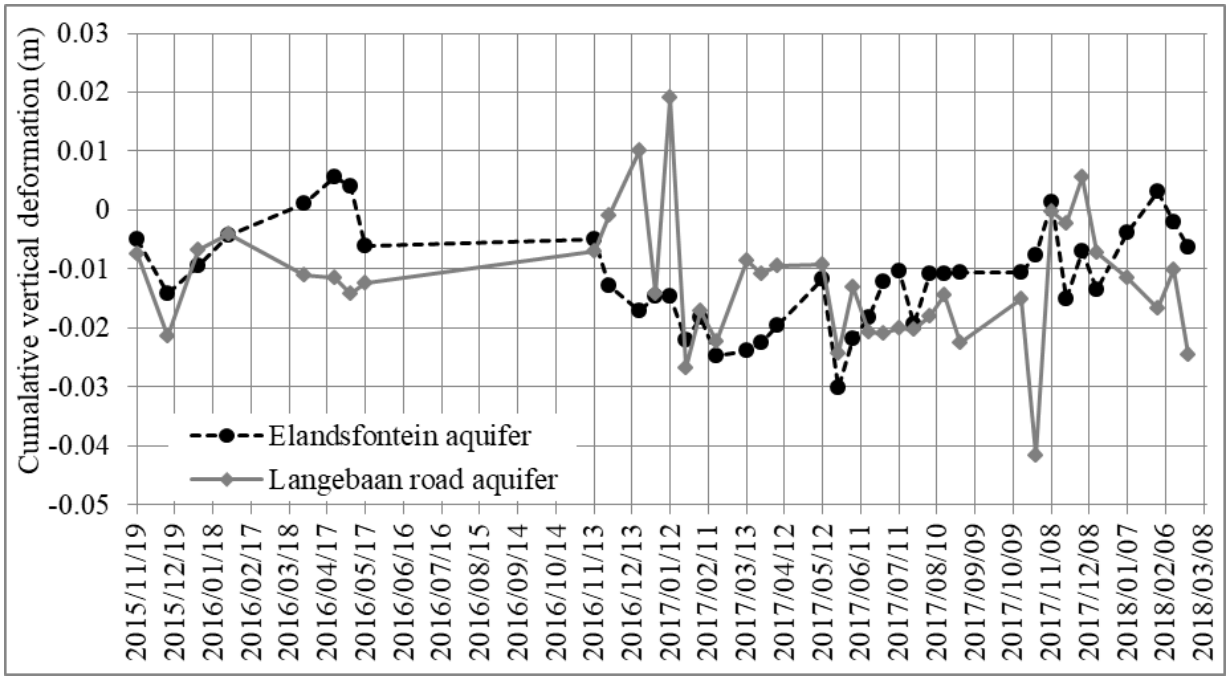

Overall, the results are rather noisy and the data not regularly sampled throughout the time series but it is noteworthy that the measurements were consistently showing subsidence. Cumulatively adding consecutive acquisitions is useful for minimising phase contributions due to atmosphere. The atmospheric delay is introduced instantaneously in one acquisition which results in an area of subsidence if the scene is used as a master, and an area of uplift when the scene is next used as a slave, a summation will cancel these contributions (Hanssen 2001). However, as certain scenes were excluded from analysis, due to failed unwrapping, the atmospheric contribution is not expected to be reliably removed using summation throughout this time series. The resulting gaps in the time series also mean that definitive conclusions about the cumulative displacement of the area over the entire time series cannot be made. Nevertheless, this is regarded as acceptable due to the exploratory nature of this study, whereby we were interested in total detectable deformation in spite of data limitations.

Another problem with cumulatively adding deformation measurements is that the result is sensitive to error propagation. The deformation rate was calculated for each borehole and averaged across each aquifer in Figure 6 to investigate the cumulative deformation results further. The standard deviations for each temporal sample of boreholes form the confidence intervals. It was necessary to convert absolute deformation to the daily deformation rate since each interferogram represents deformation

detected between image acquisitions but the time between acquisitions did not always remain constant. Figure 6 shows that interferograms with extreme values (> 0.003 m/day) have large variance and are therefore not reliable measurements and lead to bias in the cumulative displacement measurement. It should be noted that the data is well centered around 0 m, which is expected since no obvious large scale deformation has been reported for the area, and further indicating that the reference point chosen for unwrapping is reliable.

Figure 6 shows that Langebaan road had a higher variance and wider standard deviations. This result is somewhat counterintuitive as the larger sample size (n=43 compared to n=13 for Elandsfontein) is expected to result in a lower variance. The variance could be explained by the previous observation that the Langebaan road boreholes are situated between active agricultural fields that lose coherence rapidly. This is due to agricultural practises such as tilling, irrigation and seasonal plant growth and harvest cycles. It is noteworthy that the natural vegetation of the region's nature reserves may be more favourable to interferometry than semi-rural areas with more agriculture and associated infrastructure. Typically, infrastructure such as buildings, powerlines and roads provide coherent phase returns. However, due to the low resolution combined with strong multi-looking and filtering, the stable infrastructure targets (with nearby boreholes, typically found close to roads) was mixed with agricultural fields leading to coherence loss for those boreholes found close to fields.

Figure 6: Deformation rate of the Langebaan road and Elandsfontein aquifers from 2015/11/19 to 2018/02/24 measured over the department of water affairs boreholes by DInSAR.

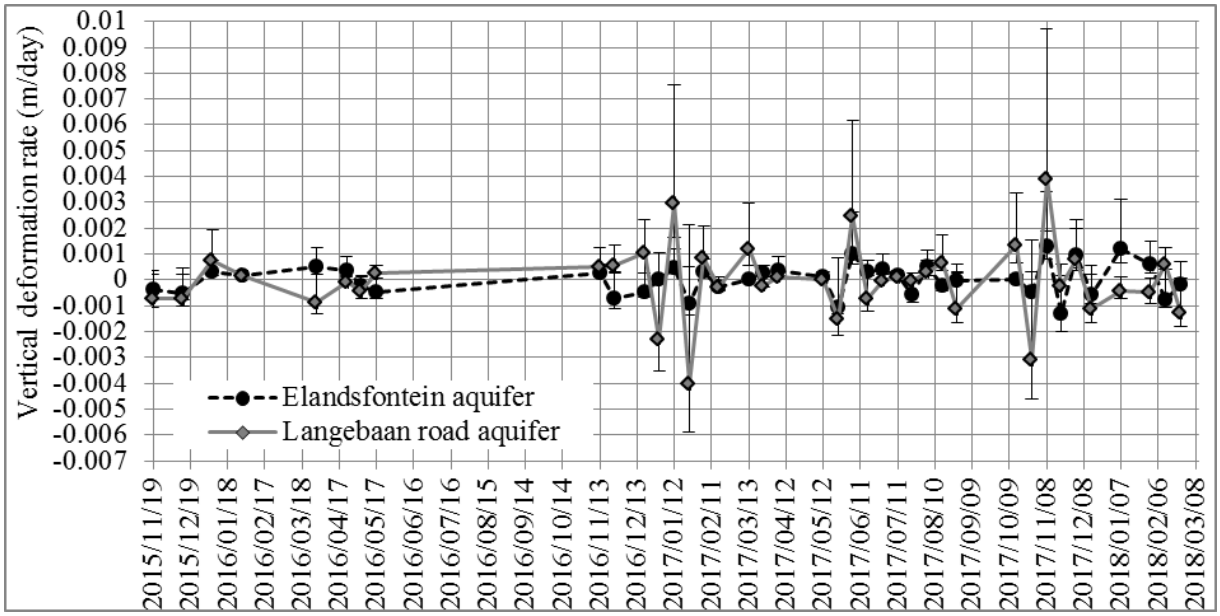

6. CONCLUSIONS AND RECOMMENDATIONS

Communities, both urban and rural, in the Western Cape are dependent on groundwater in some way. Indirectly from the food and jobs irrigated agriculture creates and increasingly directly from the drinking water abstracted from production boreholes. The aquifers in the Western Cape therefore provide a critical water resource for communities that need to be managed, particularly during the current drought and under future climate-change conditions (Department of Water Affairs 2009). The early results presented in this paper show that Sentinel-1 is an appropriate data source for monitoring aquifer related deformation in the area. However, limitations inherent to conventional DInSAR techniques were encountered namely: the dynamic land-cover of the study area leading to coherence loss, challenges in phase unwrapping, atmospheric phase contributions as well as the small magnitude of deformation. Advanced time-series techniques capable of reliably detecting small scale deformation, dealing with atmospheric phase noise and changing land use conditions are recommended for effective monitoring of aquifer related deformation in the area (Bell et al. 2008; Radutu *et al.* 2017). Finally, results should be validated with differential GPS data and compared to groundwater levels to determine if relationships between ground deformation and groundwater levels can be established to aid geo-hydrological modelling.

Acknowledgements: The authors wish to thank the CSIR Meraka Institute for providing funding through the studentship program, the European Union Copernicus program for providing the Sentinel-1 data free of charge as well as the Department of Water and Sanitation for providing the borehole location and water level data.

REFERENCE LIST

Alfarrah, N., Berhane, G., Hweesh, A. and Walraevens, K., 2017: Sinkholes Due to Groundwater Withdrawal in Tazerbo Wellfield, SE Libya, *Groundwater*, *55*(4), pp.593-601.

Amelung, F., Galloway, D.L., Bell, J.W., Zebker, H.A. and Laczniak, R.J., 1999: Sensing the ups and downs of Las Vegas: InSAR reveals structural control of land subsidence and aquifer-system deformation, *Geology*, *27*(6), pp.483-486.

Amos, C.B., Audet, P., Hammond, W.C., Bürgmann, R., Johanson, I.A. and Blewitt, G., 2014: Uplift and seismicity driven by groundwater depletion in central California, *Nature*, *509*(7501), p.483.

Armaş, I., Mendes, D.A., Popa, R.G., Gheorghe, M. and Popovici, D., 2017: Long-term ground deformation patterns of Bucharest using multi-temporal InSAR and multivariate dynamic analyses: a possible transpressional system?, *Scientific Reports*, *7*, p.43762.

Bell, J.W., Amelung, F., Ferretti, A., Bianchi, M. and Novali, F., 2008: Monitoring aquifer-system response to groundwater pumping and artificial recharge, *First break*, 26(8).

Chen, M., Tomás, R., Li, Z., Motagh, M., Li, T., Hu, L., Gong, H., Li, X., Yu, J. and Gong, X., 2016: Imaging land subsidence induced by groundwater extraction in Beijing (China) using satellite radar interferometry, *Remote Sensing*, *8*(6), p.468.

Copernicus Sentinel data 2015: Retrieved from the Sentinel hub (https://scihub.copernicus.eu/) May 2018, processed by ESA.

Costantini, M., 1998: A novel phase unwrapping method based on network programming. *IEEE Transactions on geoscience and remote sensing*, *36*(3), pp.813-821.

Department of Water Affairs 2009: Strategy and Guideline Development for National Groundwater Planning Requirements. Artificial Groundwater Recharge: Recent initiatives in Southern Africa, P RSA 000/00/11609/9 Activity 4 (AR01), dated January 2010.

Engelbrecht, J. and Inggs, M., 2015: Coherence optimisation and its limitations for deformation monitoring in agricultural regions. In *Geoscience and Remote Sensing Symposium (IGARSS), 2015 IEEE International* (pp. 1429-1432), IEEE.

Ferretti, A., Fumagalli, A., Novali, F., Prati, C., Rocca, F. and Rucci, A., 2011: A new algorithm for processing interferometric data-stacks: SqueeSAR, *IEEE Transactions on Geoscience and Remote Sensing*, *49*(9), pp.3460-3470.

Ferretti, A., Monti Guarnieri, A., Prati, C., Rocca, F. and Massonnet, D., 2007: *INSAR Principles B*. ESA publications.

Ferretti, A., Savio, G., Barzaghi, R., Borghi, A., Musazzi, S., Novali, F., Prati, C. and Rocca, F., 2007: Submillimeter accuracy of InSAR time series: Experimental validation. *IEEE Transactions on Geoscience and Remote Sensing*, *45*(5), pp.1142-1153.

Goldstein, R.M. and Werner, C.L., 1998: Radar interferogram filtering for geophysical applications, *Geophysical research letters*, *25*(21), pp.4035-4038.

Grandin, R., 2015: Interferometric processing of SLC Sentinel-1 TOPS data. In *FRINGE'15: Advances in the Science and Applications of SAR Interferometry and Sentinel-1 InSAR Workshop, Frascati, Italy, 23-27 March 2015*.

Hanssen, R.F., 2001: *Radar interferometry: data interpretation and error analysis* (Vol. 2), Kluwer Acdemic Publishers, Dordrecht.

Hooper, A., Zebker, H., Segall, P. and Kampes, B., 2004: A new method for measuring deformation on volcanoes and other natural terrains using InSAR persistent scatterers, *Geophysical research letters*, *31*(23).

Matthews S 2014: Improved groundwater monitoring through GRACE, *Water Wheel* 13, 1: 26–27.

Motagh, M., Shamshiri, R., Haghighi, M.H., Wetzel, H.U., Akbari, B., Nahavandchi, H., Roessner, S. and Arabi, S., 2017: Quantifying groundwater exploitation induced subsidence in the Rafsanjan plain, southeastern Iran, using InSAR time-series and in situ measurements, *Engineering Geology*, *218*, pp.134-151.

Niu, Z., Li, Q. and Wei, X., 2017: Estimation of the surface uplift due to fluid injection into a reservoir with a clayey interbed, *Computers and Geotechnics*, *87*, pp.198-211.

Parker A, Filmer M & Featherstone W 2017. First Results from Sentinel-1A InSAR over Australia: Application to the Perth Basin. Remote Sensing 9, 3: 299.

Pepler AL 2013: Elandsfontein phosphate project: Geology and Resource Statement, draft report Elandsfontein Exploration and Mining (Pty) Ltd.

Du Plessis, J.A., 2009: Managing the unseen: Langebaan road aquifer system, *Water SA*, *35*(2), pp.152-157.

Radutu, A., Nedelcu, I. and Gogu, C.R., 2017: An overview of ground surface displacements generated by groundwater dynamics, revealed by InSAR techniques, *Procedia engineering*, *209*, pp.119-126.

Rezaei, A., 2018: Comments on “Quantifying groundwater exploitation induced subsidence in the Rafsanjan plain, southeastern Iran, using InSAR time-series and in situ measurements” by Motagh, M., Shamshiri, R., Haghighi, MH, Wetzel, HU, Akbari, B., Nahavandchi, H., & Arabi, S.[Engineering Geology, 218 (2017), 134–151]. *Engineering Geology*.

South Africa 1998. National water act, Act 36 of 1998. Government Gazette of South Africa, 19182,1091 398,1999.

Theron, A., 2017: Detection of sinkhole precursors through SAR interferometry, Unpublished M.Sc. Dissertation, Stellenbosch University, Stellenbosch.

Wang, Y.Q., Wang, Z.F. and Cheng, W.C., 2018: A review on land subsidence caused by groundwater withdrawal in Xi’an, China, *Bulletin of Engineering Geology and the Environment*, pp.1-13.

Wegmüller, U., Werner, C., Strozzi, T., Wiesmann, A., Frey, O. and Santoro, M., 2015: September. Sentinel-1 IWS mode support in the GAMMA software, In *Synthetic Aperture Radar (APSAR), 2015 IEEE 5th Asia-Pacific Conference on* (pp. 431-436). IEEE.

Western Cape Department of Agriculture 2017: Informing the Western Cape agricultural sector on the 2015-2017 drought, Western Cape Government, Cape Town.

Master date	Slave date	Temporal Baseline (days)	Perpendicular baseline (m)	Quality check	Reference Offset (m)	Master date	Slave date	Temporal Baseline (days)	Perpendicular baseline (m)	Quality check	Reference Offset (m)
2015/11/19	2015/12/01	12	-61	pass	-0.0159	2017/05/12	2017/05/24	12	43	pass	-0.0032
2015/12/01	2015/12/13	12	-76	fail	n/a	2017/05/24	2017/06/05	12	-6	pass	0.0016
2015/12/13	2016/01/06	24	108	pass	-0.0015	2017/06/05	2017/06/17	12	67	pass	0.0180
2016/01/06	2016/01/30	24	50	pass	-0.0262	2017/06/17	2017/06/29	12	1	pass	0.0064
2016/01/30	2016/02/23	24	-114	pass	0.0131	2017/06/29	2017/07/11	12	-34	pass	0.0086
2016/02/23	2016/03/18	24	79	fail	n/a	2017/07/11	2017/07/23	12	-1	pass	0.0065
2016/03/18	2016/03/30	12	28	fail	n/a	2017/07/23	2017/08/04	12	-49	pass	-0.0050
2016/03/30	2016/04/11	12	19	pass	0.0049	2017/08/04	2017/08/16	12	76	pass	0.0162
2016/04/11	2016/04/23	12	62	fail	n/a	2017/08/16	2017/08/28	12	-25	pass	0.0104
2016/04/23	2016/05/05	12	22	pass	0.0187	2017/08/28	2017/09/09	12	-25	pass	0.0094
2016/05/05	2016/05/17	12	39	pass	-0.0173	2017/09/09	2017/09/21	12	-22	fail	n/a
2016/05/17	2016/06/10	24	11	pass	-0.0028	2017/09/21	2017/10/03	12	37	fail	n/a
2016/06/10	2016/11/13	156	-70	fail	n/a	2017/10/03	2017/10/15	12	16	fail	n/a
2016/11/13	2016/11/25	12	7	pass	0.0109	2017/10/15	2017/10/27	12	-24	pass	-0.0083
2016/11/25	2016/12/07	12	19	pass	0.0127	2017/10/27	2017/11/08	12	24	pass	-0.0091
2016/12/07	2016/12/19	12	-15	fail	n/a	2017/11/08	2017/11/20	12	-63	pass	-0.0193
2016/12/19	2016/12/31	12	-87	pass	-0.0044	2017/11/20	2017/12/02	12	38	pass	0.0101
2016/12/31	2017/01/12	12	23	pass	0.0040	2017/12/02	2017/12/14	12	14	pass	-0.0096
2017/01/12	2017/01/24	12	74	pass	-0.0066	2017/12/14	2017/12/26	12	71	pass	0.0128
2017/01/24	2017/02/05	12	22	pass	0.0006	2017/12/26	2018/01/07	12	-53	fail	n/a
2017/02/05	2017/02/17	12	50	pass	0.0059	2018/01/07	2018/01/19	12	-86	pass	-0.0061
2017/02/17	2017/03/13	24	-116	pass	0.0082	2018/01/19	2018/01/31	12	38	fail	n/a
2017/03/13	2017/03/25	12	44	pass	-0.0127	2018/01/31	2018/02/12	12	-18	pass	-0.0078
2017/03/25	2017/04/06	12	34	pass	0.0062	2018/02/12	2018/02/24	12	117	pass	0.0048
2017/04/06	2017/04/18	12	4	pass	0.0247	2018/02/24	2018/03/08	12	49	pass	0.0178
2017/04/18	2017/04/30	12	-9	fail	n/a	2018/03/08	2018/03/20	12	-52	fail	n/a
2017/04/30	2017/05/12	12	-84	fail	n/a	2018/03/20	2018/04/01	12	-76	fail	-0.0187

List of figures:

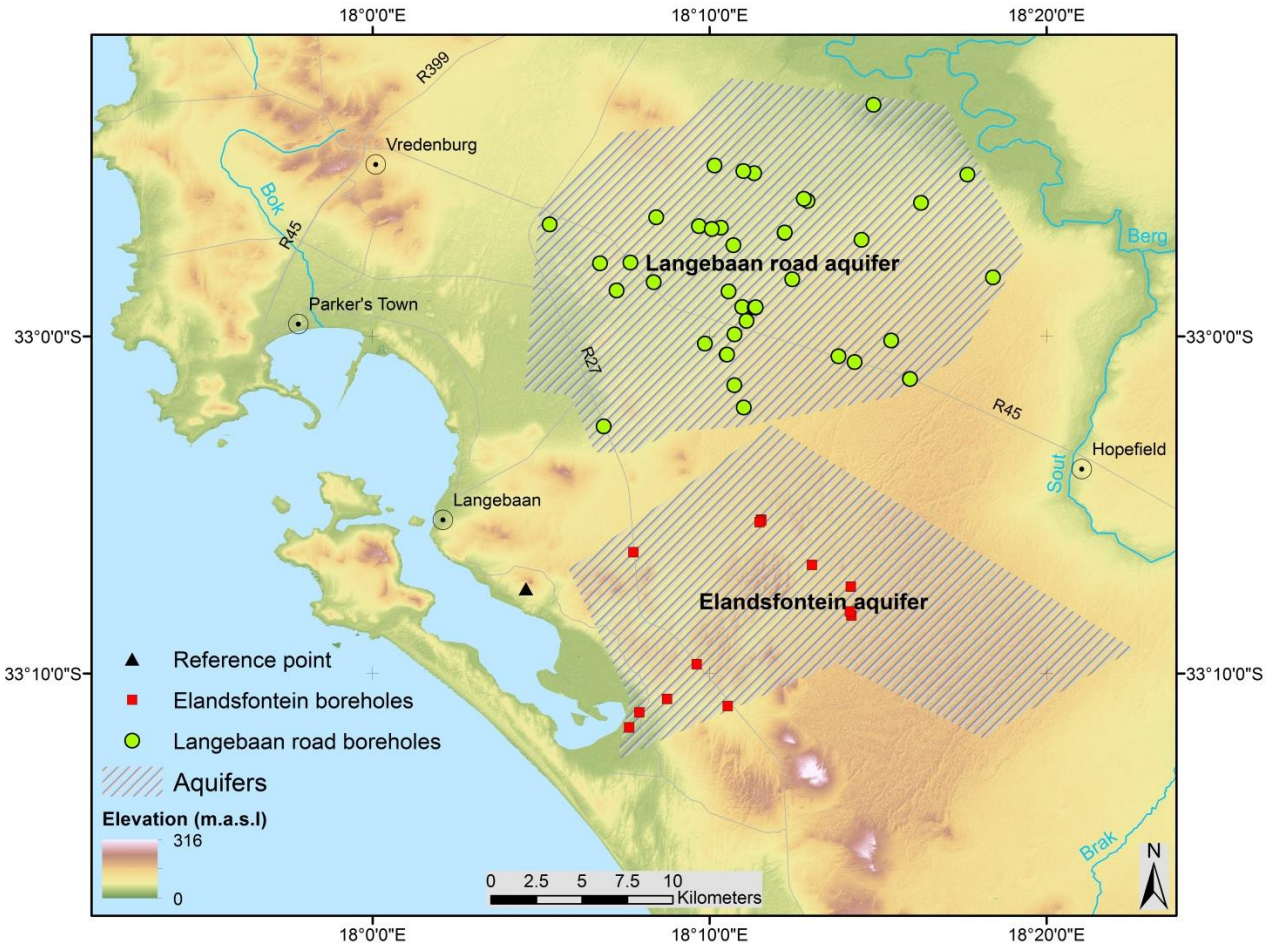
18°0'0"E
18°10'0"E
18°20'0"E
33°0'0"S
33°10'0"S
R399
Vredenburg
Bok
R45
Parker's Town
Langebaan road aquifer
Berg
R27
R45
Hopefield
Sout
Langebaan
Elandsfontein aquifer
Reference point
Elandsfontein boreholes
Langebaan road boreholes
Aquifers
Elevation (m.a.s.l)
316
0
0 2.5 5 7.5 10
Kilometers
Brak
N

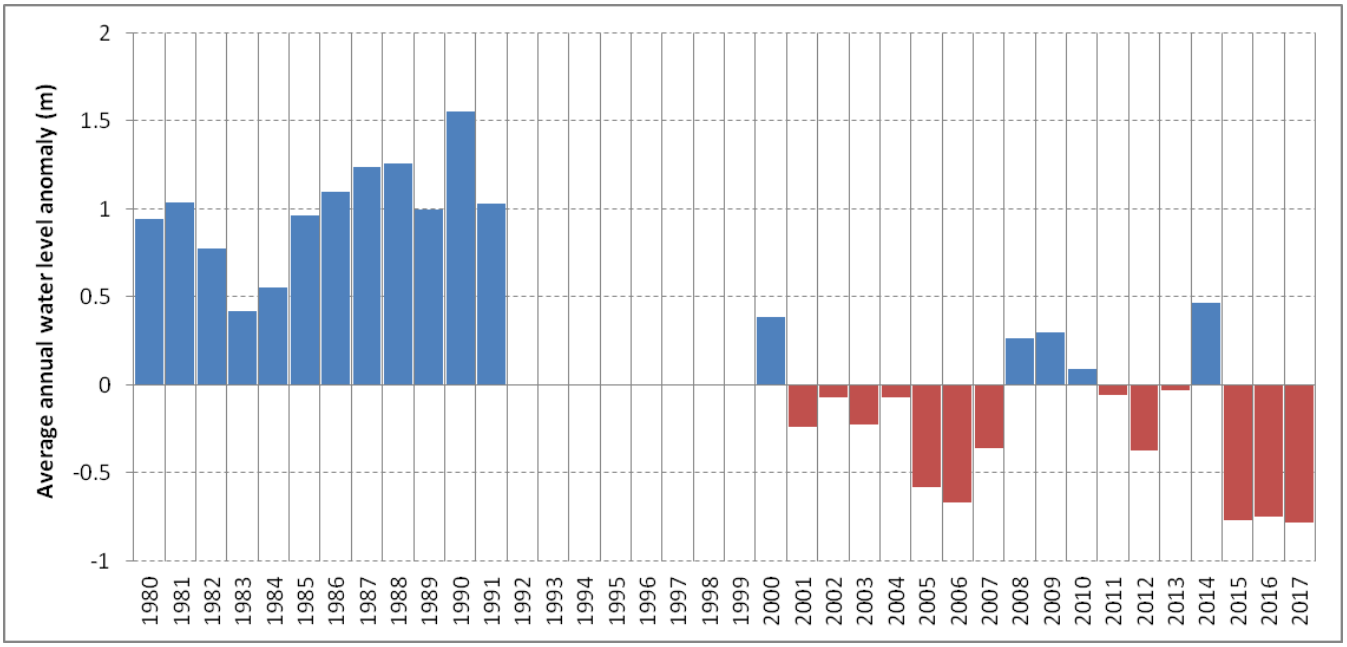
Average annual water level anomaly (m)
2
1.5
1
0.5
0
-0.5
-1
1980
1981
1982
1983
1984
1985
1986
1987
1988
1989
1990
1991
1992
1993
1994
1995
1996
1997
1998
1999
2000
2001
2002
2003
2004
2005
2006
2007
2008
2009
2010
2011
2012
2013
2014
2015
2016
2017

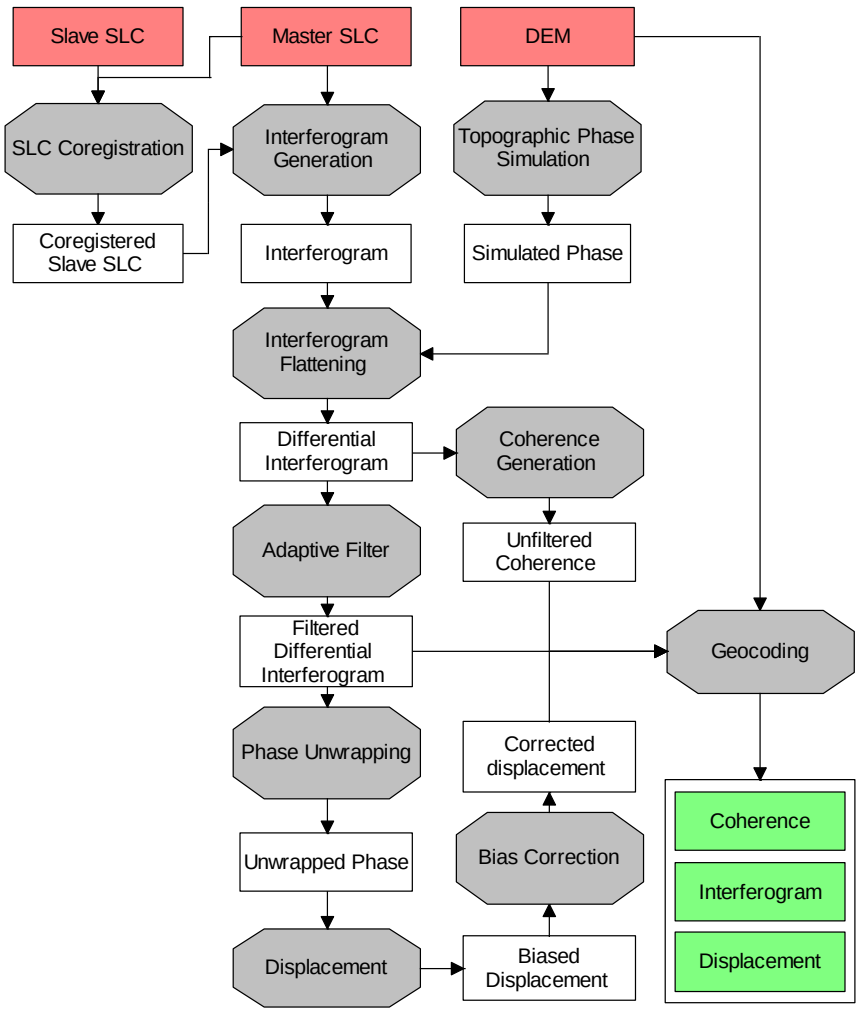
Slave SLC
Master SLC
DEM
SLC Coregistration
Interferogram Generation
Topographic Phase Simulation
Coregistered Slave SLC
Interferogram
Simulated Phase
Interferogram Flattening
Differential Interferogram
Coherence Generation
Adaptive Filter
Unfiltered Coherence
Filtered Differential Interferogram
Geocoding
Phase Unwrapping
Corrected displacement
Coherence
Unwrapped Phase
Bias Correction
Interferogram
Displacement
Biased Displacement
Displacement

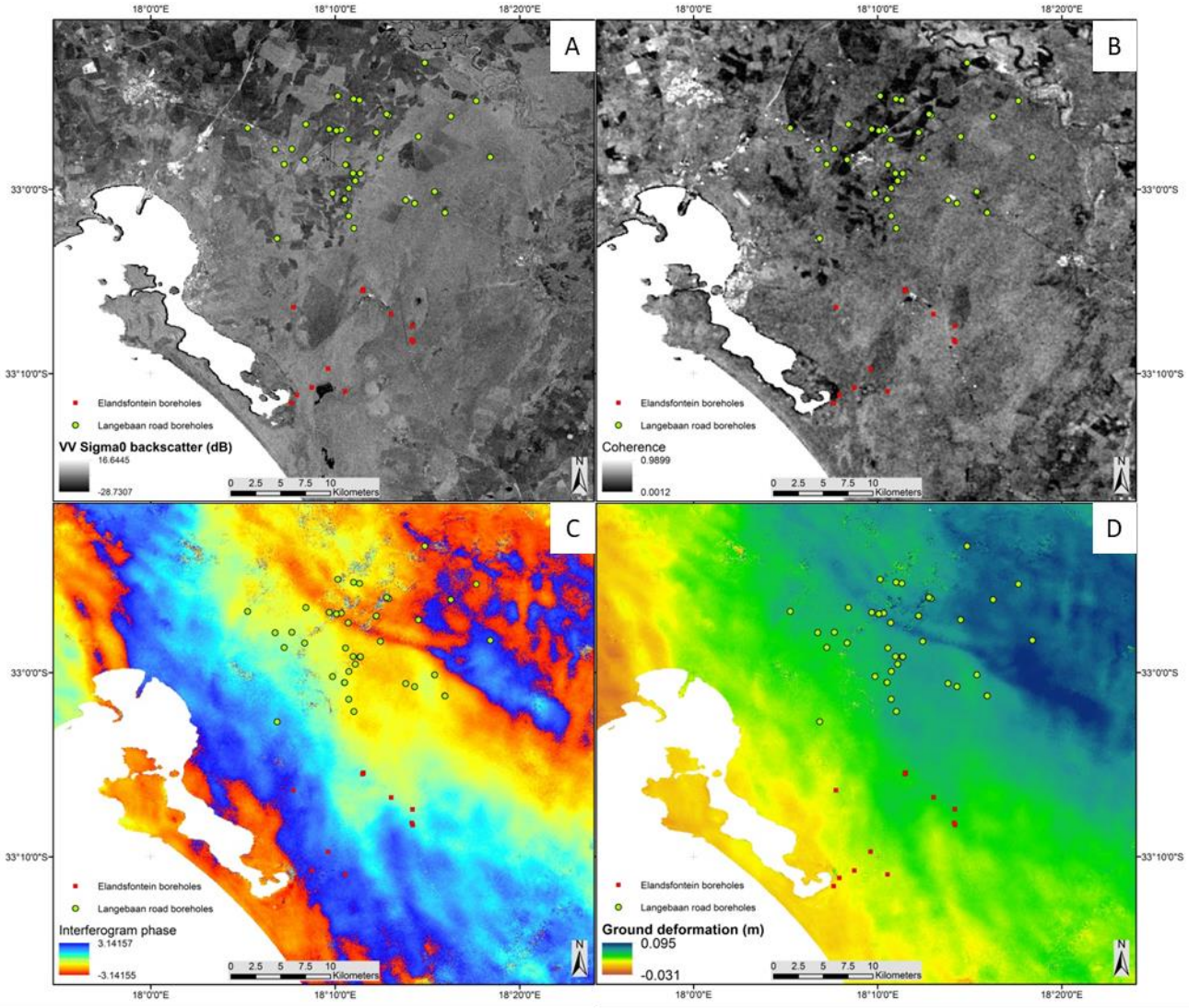
A
B
C
D
18°0'0"E
18°10'0"E
18°20'0"E
33°0'0"S
33°10'0"S
Elandsfontein boreholes
Langebaan road boreholes
VV Sigma0 backscatter (dB)
16.6445
-28.7307
Coherence
0.9899
0.0012
Interferogram phase
3.14157
-3.14155
Ground deformation (m)
0.095
-0.031
0 2.5 5 7.5 10
Kilometers
N

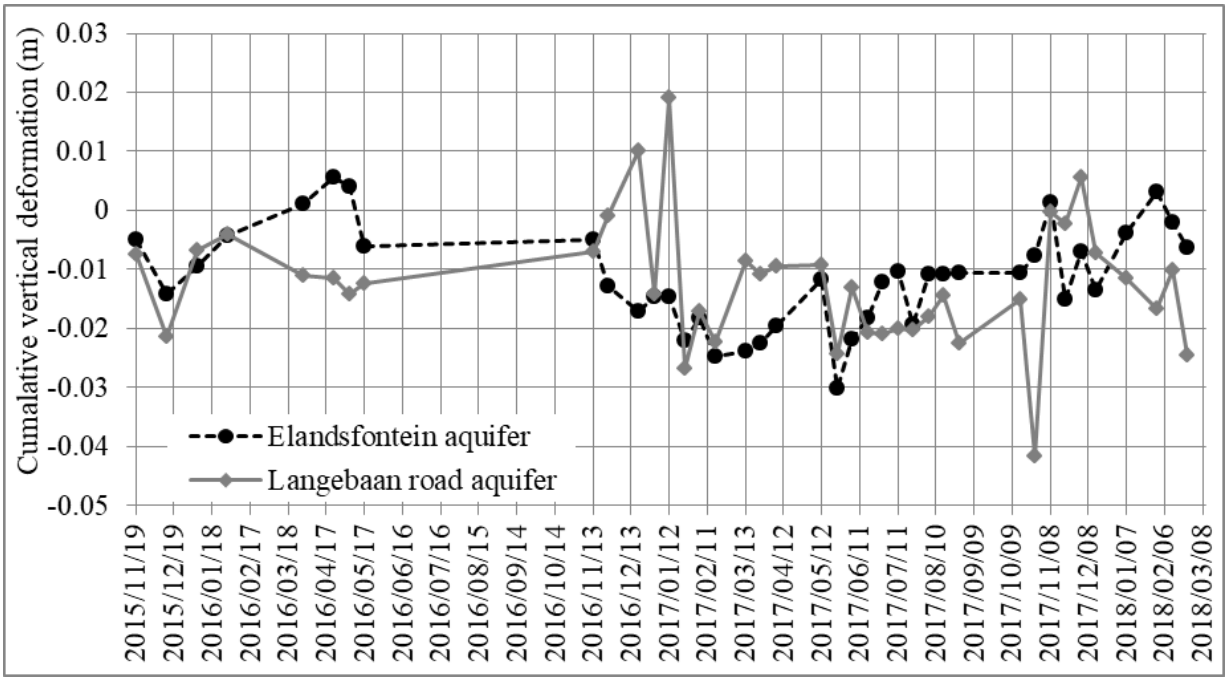
Cumalative vertical deformation (m)
0.03
0.02
0.01
0
-0.01
-0.02
-0.03
-0.04
-0.05
Elandsfontein aquifer
Langebaan road aquifer
2015/11/19
2015/12/19
2016/01/18
2016/02/17
2016/03/18
2016/04/17
2016/05/17
2016/06/16
2016/07/16
2016/08/15
2016/09/14
2016/10/14
2016/11/13
2016/12/13
2017/01/12
2017/02/11
2017/03/13
2017/04/12
2017/05/12
2017/06/11
2017/07/11
2017/08/10
2017/09/09
2017/10/09
2017/11/08
2017/12/08
2018/01/07
2018/02/06
2018/03/08

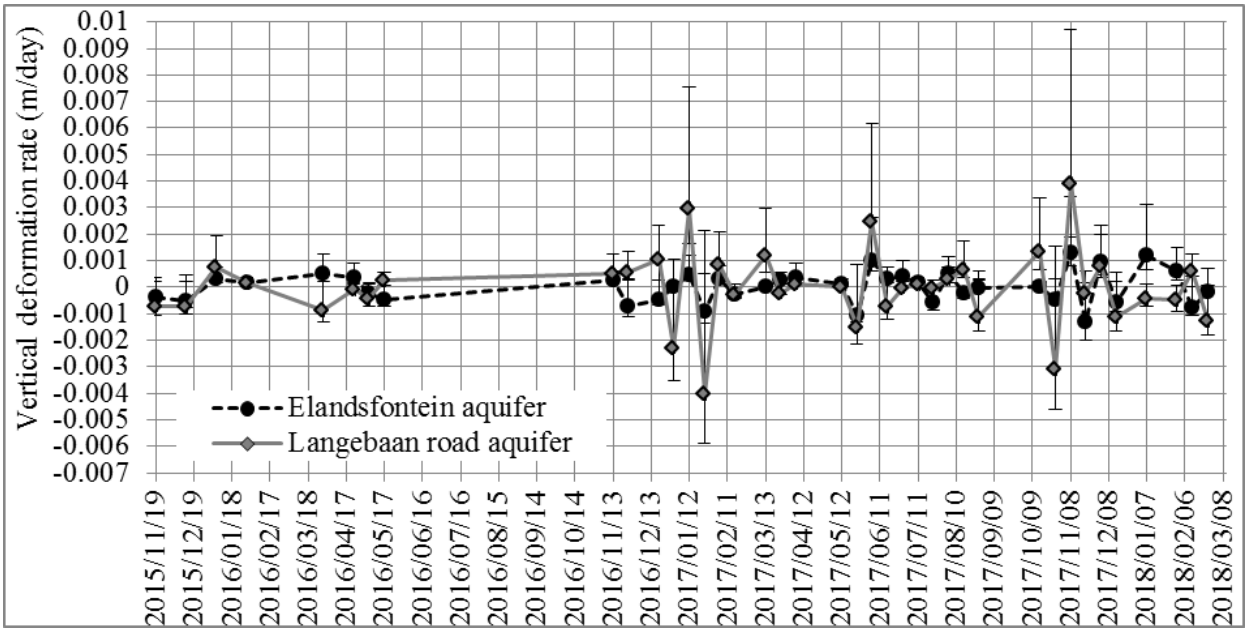
Vertical deformation rate (m/day)
0.01
0.009
0.008
0.007
0.006
0.005
0.004
0.003
0.002
0.001
0
-0.001
-0.002
-0.003
-0.004
-0.005
-0.006
-0.007
Elandsfontein aquifer
Langebaan road aquifer
2015/11/19
2015/12/19
2016/01/18
2016/02/17
2016/03/18
2016/04/17
2016/05/17
2016/06/16
2016/07/16
2016/08/15
2016/09/14
2016/10/14
2016/11/13
2016/12/13
2017/01/12
2017/02/11
2017/03/13
2017/04/12
2017/05/12
2017/06/11
2017/07/11
2017/08/10
2017/09/09
2017/10/09
2017/11/08
2017/12/08
2018/01/07
2018/02/06
2018/03/08